JOURNAL OF AIRCRAFT
Vol. 29, No. 6, Nov.–Dec. 1992

Physical Modeling of Ground Effects on Vortex Wakes

H.-T. Liu,* P. A. Hwang,† and R. A. Srnsky‡
QUEST Integrated, Inc., Kent, Washington 98032

Towing-tank experiments were conducted to investigate ground effects on vortex wakes. Two methods were used to generate the vortex wakes: 1) a towed NACA 0012 wing and 2) a slotted-jet vortex generator. Trajectories derived from trailing vortex wakes, tagged with a fluorescent dye and released near the simulated ground surface, have confirmed the inadequacy of the two-dimensional inviscid solution. The generation of a relatively weak secondary vortex causes the primary vortex to rebound from the surface as a result of unsteady separation. There is no significant difference between the trajectories, whether the ground is simulated by a rigid surface or a free surface. The introduction of a rigid surface close to the exit of the slotted-jet vortex generator results in the formation of secondary vortices at the ground outboard of the primary vortices. The secondary vortices generated by the slotted-jet vortex pair are more coherent and persistent than those generated by the trailing vortex pair. A simple modification of the two-dimensional inviscid theory—namely, adding a secondary vortex to the system—recreates the rebound phenomenon, which agrees qualitatively with the trend seen in the experiments.

Nomenclature

b_0 = separation of a trailing vortex pair as derived from inviscid theory, $S\pi/4$
b_∞ = asymptotic vortex separation for y and z approaching infinity
h = depth of vortex cores to the mean water surface
h_s = initial release depth of the vortex pair
h_{max} = maximum vertical translation defined in Eq. (5)
r = instantaneous distance of vortex center from the origin, $r = (y^2 + z^2)^{1/2}$
r' = distance between the primary and secondary vortices
S = wing span
t = time
W_0 = initial downwash velocity of vortex translation
y = horizontal axis
y_0 = one-half of the initial vortex separation
z = vertical axis ($z = 0$ is the free surface)
θ' = rotation angle of the primary and secondary vortices
κ = circulation of primary vortices
κ' = circulation of secondary vortices

Introduction

THE volume of air traffic at major airports has been increasing at an alarming rate without any sign of relief. One method of easing air traffic congestion is to minimize the separation times, or distances, between airplanes for takeoffs and landings. Since light aircraft passing through strong wakes may experience difficulties in maintaining control, aircraft separation at congested airports is dictated by the characteristics of the vortex wakes left behind by larger aircraft. At present, one of the least understood vortex phenomena is the behavior of a vortex wake released near the ground, which presents an obstacle for minimizing the safe separation between airplanes.

The greatest impact of the vortex wake of a large aircraft on smaller followers, is near ground level (<60 m), where the smaller aircraft may not have sufficient time or space to recover from the influence of the swirl in the wake. Also, the ground plays an important role in modifying the trajectory of the vortex wake during takeoff and landing. The ground surface acts as a reflection plane, and the motion of the vortex pair is determined not only by the mutual induction of the vortices, but also by the image vortex pair below the ground surface. In other words, the trajectory of the ideal vortices is determined by the mutual induction of four vortices. Lamb[1] has shown that the trajectories of line vortices in an ideal fluid are hyperbolas given by

$$y^{-2} + z^{-2} = 4b_\infty^{-2} \tag{1}$$

For an elliptically loaded wing, the vortex separation in the absence of ground effect is $b_0 = S\pi/4$. Dimensionless parameters are often formed using b_0 and W_0 as the length and velocity scales. For example, Eq. (1) may be expressed in dimensionless form as

$$(y/b_0)^{-2} + (z/b_0)^{-2} = 4(b_\infty/b_0)^{-2} \tag{2}$$

The plane $y/b_0 = 0$ corresponds to the plane of symmetry between the two vortex elements. For a vortex pair with an initial separation of $2y_0/b_0$ released at $z_0/b_0 = h_s/b_0$, the asymptotic vortex separation may be derived from Eq. (2) as

$$b_\infty/b_0 = 2[(y_0/b_0)^{-2} + (h_s/b_0)^{-2}]^{-0.5} \tag{3}$$

If b_∞ instead of b_0 is chosen as the length scale to form the dimensionless variables, Eq. (2) may be written as

$$(y/b_\infty)^{-2} + (z/b_\infty)^{-2} = 4 \tag{4}$$

Both Eqs. (2) and (4) show that the two vortices turn sideways as they approach the ground. The asymptotic distance between the surface and the vortex released initially at h_s/b_0 is $b_\infty/b_0/2$. In other words, the vortex pair does not come closer to the surface than a distance of half the asymptotic vortex separation. Alternatively, Eqs. (2) and (4) may be expressed in terms of the vertical vortex translation h/b_0 by substituting z/b_0 with $h_s/b_0 - h/b_0$. The maximum vertical translation or height of the vortex wake is then

$$h_{max}/b_0 = h_s/b_0 - b_\infty/b_0/2 \tag{5}$$

Received June 14, 1991; revision received Oct. 31, 1991; accepted for publication Oct. 31, 1991.

*Principal Scientist, Applied Physics Division. Member AIAA.
†Senior Scientist, Applied Physics Division.
‡Supervisor, Fluid Mechanics Laboratory.

Initially, as the vortex wake approaches the ground, Eq. (1) or (4) is in general agreement with flight data.[2,3] Subsequently, the flight data display a consistent trend of deviation from the two-dimensional theoretical trajectory in that the vortices rise again after having descended close to the ground. In a related problem of a rising vortex pair approaching a free surface in a towing tank, Sarpkaya and Johnson[4] observed a rebound of vortices similar to that shown in the flight data. They suggested that the sidewalls may be responsible, which obviously cannot explain the flight data in the absence of any sidewall.

In an attempt to explain the above phenomenon, Harvey and Perry[3] conducted an experiment using a half-span wing to generate a single vortex passing over a moving floor in a wind tunnel. From the total head measurement, they inferred the following scenario. The passage of the primary vortex induces a crossflow on the ground with an attendant suction peak beneath the vortex core. Consequently, the crossflow boundary layer has to negotiate an adverse pressure gradient once it has passed under the vortex. When the vortex is sufficiently near the ground, the adverse pressure gradient is strong enough for separation from the boundary layer to occur, and a separation bubble forms containing vorticity opposite to the main vortex. The bubble grows rapidly and finally detaches from the ground, forming a secondary vortex, which remains outboard of the primary vortex. One of the effects of the secondary vortex is to induce an upward movement of the primary vortex.

In another study, Bilanin et al.[5] incorporated a viscous ground plane in a second-order closure turbulence model to simulate the ground/vortex interaction. The numerical solution demonstrated the growth and separation of the boundary layer beneath the approaching vortex, resulting in a counter-rotating secondary vortex. The secondary vortex induces an upward and outward motion on the approaching vortex, leading to the rebounding phenomenon. Furthermore, the results of this study have shown that rebound is more prominent in a laminar, than in a turbulent, boundary layer. One of the most important findings is that the rebounding phenomenon does not occur unless the viscous boundary-layer condition is applied. This indicates that the rebound is not attributable to the effects of a finite vortex core radius as suggested by Barker and Crow.[6]

Didden and Ho[7] experimentally investigated the impingement of a jet on a flat plate. The jet was conditioned to shed a series of primary vortices that impinge upon the plate. From velocity profiles measured with hot-wire probes, it was demonstrated that the perturbations of the primary vortex in the inviscid region create an unsteady adverse wall pressure gradient slightly ahead of the primary vortex core, which retards the flow in the viscous local shear layer at the viscous-inviscid interface. The vorticity in the shear layer combines to form a secondary vortex and protrudes into the inviscid region, leading to unsteady separation. The generation of the secondary vortex has been confirmed computationally using the method of large-eddy simulations.[8]

Another experimental study investigated the effects of surface contamination on the rebound of slotted-jet vortex pairs in a water tank.[9] It was demonstrated that surface contamination, such as by dust and surface active agents, effectively causes the free surface to act like a solid surface during vortex impingement. Only an extremely clean surface (which is practically nonexistent) would fulfill the free-surface boundary condition.

This article describes the results derived from several series of towing-tank experiments with emphasis on the rebound of primary vortices due to ground effect, which is not well understood, yet extremely important, for airport traffic control and safety operations. These results shed some light on the complex phenomenon of viscous-inviscid interactions and will be valuable in the development of accurate predictive models for use in airport operations.

Technical Approach and Experimental Methods

This section describes the technical approach and experimental methods used to simulate the ground effects on the behavior of a vortex wake in a towing tank. The use of a towing tank has been demonstrated to be most suitable for studying the evolution of vortex wakes.[4,10] The simulated vortex phenomenon has the same spatial and temporal references as those of airplane wakes, and ground effects on the vortex evolution may be easily simulated under different atmospheric conditions.

The towing tank system used in this study is 18.3-m-long, 1.2-m-wide, and 0.91-m-high. It has glass sidewalls and floor to permit visualization from all directions. A description of the towing tank system for physically modeling vortex phenomena is given elsewhere.[10]

Vortex wakes were generated using two different methods: 1) a rectangular wing model (NACA 0012) towed along the axis of the tank; and 2) a slotted-jet vortex generator with its axis perpendicular to that of the tank. The NACA 0012 wing model has a 10.2-cm span and a 5.1-cm chord. The maximum dimensions of the wing are dictated by the dimensions of the towing tank and the requirement that interference of the water surface, the tank floor, and the tank walls on the vortex wake be minimized. For a towing speed of 40 cm/s, the chord Reynolds number is 20,400. The wing was set at -10 deg for all the runs. Instead of using a strut or sting, a special mounting technique was used to suspend the wing with three thin, stainless-steel wires (0.008–0.013 cm in diameter). This eliminated any flow interference by the strut or sting, which would interact with and possibly contaminate the vortex wake during its evolution. For a detailed description of the wing and its performance, such as its stability during tow, refer to Liu.[10]

Ground effects on the vortex trajectories were simulated by placing the NACA 0012 wing below the water surface at -10 deg incidence; several depths were tested. This setup corresponds to an inverted model of a vortex wake generated by an aircraft flying near the ground at a constant altitude. Strictly speaking, a free water surface behaves differently from a solid surface. To simulate a rigid surface in the towing tank, the water surface was covered with rigid foam sheets, leaving a narrow gap (10–15 cm or $1.25-1.9b_0$ wide) directly above the wing to clear the suspension wires. From the visual records, it can be seen that the vortices quickly separate beyond the width of the gap, so the gap has little effect on the rebound process. In a few cases, the water was left free to enable visualization of both the top and end views of the vortex wake. These tests also allow comparison of differences in ground effects that are attributable to different surface types.

The second vortex-generation method used in this study is a slotted-jet vortex generator that operates by ejecting fluid out of a box through a narrow slot. This vortex generator consists of a sealed box with a slot 5.7-cm-wide and 120-cm-long (the same as the tank width) on its bottom side; the edges of the slot have a 45 deg bevel. The box is made of aluminum with dimensions of 18 cm (width) by 32 cm (depth). The bottom of the box is submerged below the water surface, and the vortex pair is formed and exits from the slot. The water level in the box is lifted by means of a vacuum pump. Compressed air is supplied by a large shop compressor. A pressure line is connected to a paint tank that is partially filled with water; a separate pressure line connects the paint tank and the generator box. The volume of water in the tank is inversely proportional to the pressure used to drive the vortex generator.

The vortex pair cannot be generated simply by using a plunger that starts and stops impulsively. An impulsive stop creates a counter-rotating vortex pair (as opposed to the pair generated by an impulsive start) that tends to annihilate the motion of the primary vortex pair. To eliminate the impulsive stop, the above plunging mechanism was designed using compressed air as the forcing medium. With this design, it is possible to generate a constant pressure stroke for an ad-

justable period of time and then a ramped-down pressure stroke, achieving a "soft stop." The soft stop prevents the generation of the counter-rotating vortex pair.

The ejection of fluid is controlled through a timing circuit by two solenoid valves on the paint tank. One valve is on the inlet to the paint tank, and the other is between the vortex box and the paint tank. Typically, the paint tank is pressurized to 20 psi. To trigger an event, a switch activates the timing circuit, which opens both solenoid valves. This initiates a strong, continuous supply of air that forces the fluid through the slot. After 2 s, the supply valve closes. This gradually halts the ejection by having the residual air in the paint tank slowly reduce to atmospheric level. After 15 s, the solenoid valve to the vortex box closes.

Fluorescent dye illuminated by a laser sheet was used to trace the vortex wakes.[10] In the towed-wing experiments, a thin paste of fluorescent dye (e.g., fluorescein disodium salt) mixed in corn syrup was spread onto the side edges of the wing. Visualization of the end view was achieved by illuminating a plane perpendicular to the axis of the tank with a sheet of laser light (5 W argon laser) generated by projecting the laser beam onto an oscillating mirror. Cameras were placed outside the tank at about 30 deg from the tank axis. Corrections were applied to measurements of the vortex trajectories to account for any distortion due to the perspective angle. For the slotted-jet vortex pair, a neutrally buoyant fluorescent dye solution was suspended in the vortex generator just above the slot. The dye was carried into the vortex pair to serve as the tracer for visualization. A sheet of laser light perpendicular to the axis of the generator illuminated the vortex pair. Yardsticks were placed inside the tank to record the length scale on film for calibration and correction during image processing.

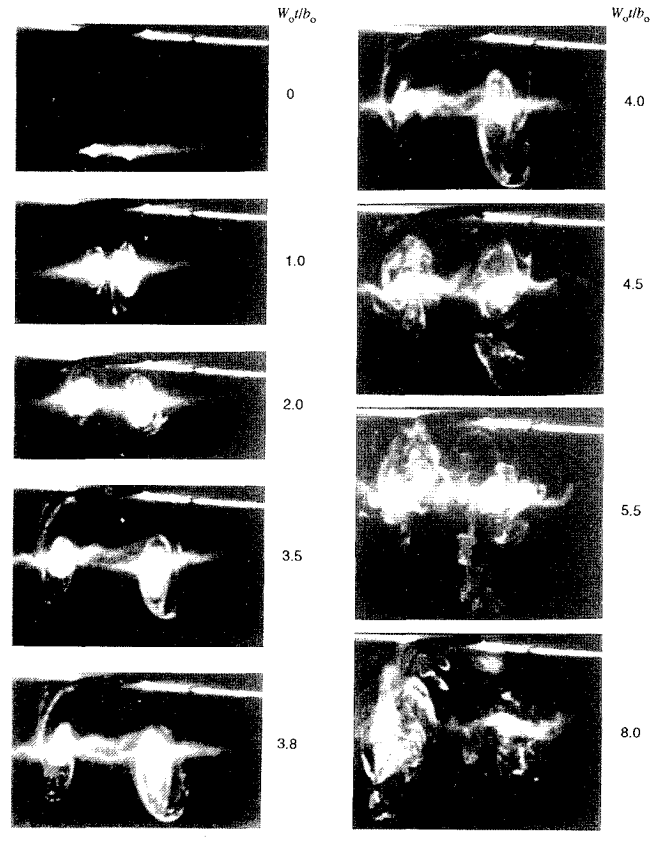

Fig. 1 Visual results of a trailing vortex pair released close to a covered water surface (white lines), $h_s/b_0 = 1.9$.

Results

Trailing Vortex Wake

Visualization

Figure 1 is a series of photographs excerpted from a movie record showing the end view (30 deg from the vortex axis) of a trailing vortex wake approaching and rebounding from a covered surface $1.9b_0$ above the wing; refer to Liu[10] for a comparison of the visual results in the absence of ground effects. The dimensionless time W_0t/b_0 is shown on the side of each photograph; the initial nondimensional depth h_s/b_0 was 1.9. The appearance of the vortex elements at any instant and location may vary depending on how much dye was entrained to track the cores and recirculation regions. Note that the vortex cores upstream and downstream of the illuminated plane are also visible as a result of a secondary fluorescent effect. The covered surface is identified by a bright line above the vortices. In the photograph series, the evolution of the secondary vortex from the primary vortex can be seen; this can be seen most distinctly in the right side primary vortex, which shows a relatively clear pattern.

At $W_0t/b_0 = 0$, the vortex pair appears as two tightly wound thin cores that expand as the dye diffuses into the recirculation region. As the vortex pair moves upward, the vortex separation begins to increase ($W_0t/b_0 > 1$) as the water surface is felt. In the absence of dye outside the primary vortex, the initial generation of a secondary vortex at the water surface outboard of the primary vortex is not visible. The secondary vortex only becomes identifiable after dye from the primary vortex is entrained into the newly formed recirculation cell (but not the cores) and outlines the structure. The generation and evolution of the secondary vortex is convincingly illustrated for the slotted-jet vortex pair as shall be seen. At $W_0t/b_0 = 2$, the secondary vortex is barely identifiable outboard to the right of the primary vortex. Subsequently, the secondary vortex is outlined by the dye spirals around the primary vortex ($2 < W_0t/b_0 < 4$) and finally turns into a turbulent patch that separates further from the primary vortex ($W_0t/b_0 > 4$) and disintegrates. This action indicates that the secondary vortex is weaker in strength than its primary counterpart. Similar evolution patterns are observed in a test run with a free water surface as shown in Fig. 2. The strength of the secondary vortices is comparable for the two runs. As demonstrated by Bernal et al.,[9] surface contamination causes the free surface to act like a rigid surface.

These visual results confirm the scenario inferred by Harvey and Perry.[3] The same phenomenon has also been seen in the results of experimental and numerical modeling studies of a jet impinging onto a fixed wall.[7,8] The authors of these studies attributed the formation of the secondary vortices to the unsteady separation of the wall boundary layer caused by an adverse pressure gradient, again reinforcing the visual results presented here.

Vortex Trajectories

The trajectories of the vortex wakes were derived from the visual results. Figures 3 and 4 compare the vertical translation, h/b_0, and the vortex separation, b/b_0, respectively, in the presence of a covered surface (CS) and a free surface (FS) for $h_s/b_0 = 1.9$ (three runs) and 0.64 (two runs). Note that W_0 decreases with decreasing h_s, a well-known ground effect that results in lift reduction. Once generated, the vortex wakes rise toward the surface, reach the maximum translations, and then rebound. The closer the wing to the surface, the smaller the maximum translation, and the sooner it is reached. For $h_s/b_0 = 1.9$, there is a relatively gentle transition as the vortex wake rebounds. For $h_s/b_0 = 0.64$, on the other hand, the transition is abrupt and the rebound is nearly specular. In spite of the differences in the two surface conditions, the trajectories of the vortex wakes show reasonably good agreement as the wakes approach the surface and rebound for some distance. Further downstream, vortex bursting as the result of instability is evident,[10,11] and the similarity deteriorates. Comparison of the vertical translations shows that good agree-

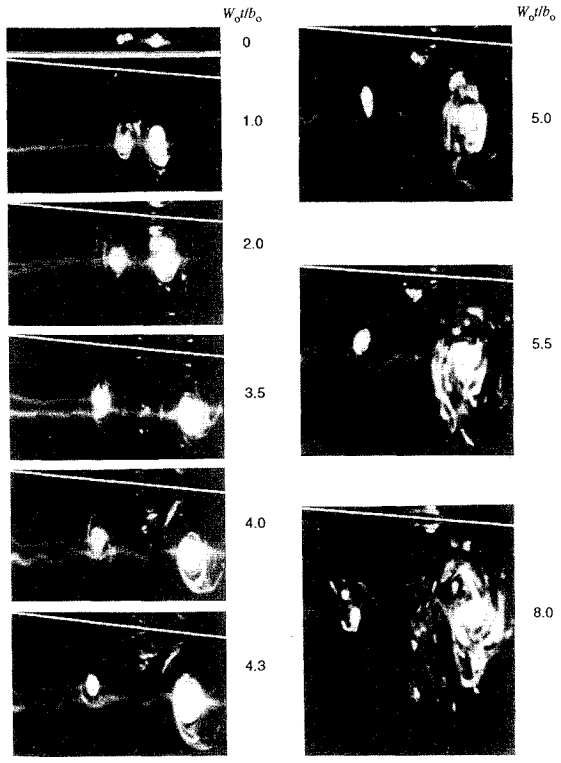

Fig. 2 Visual results of a trailing vortex pair released close to a free-water surface (white lines), $h_s/b_0 = 1.9$.

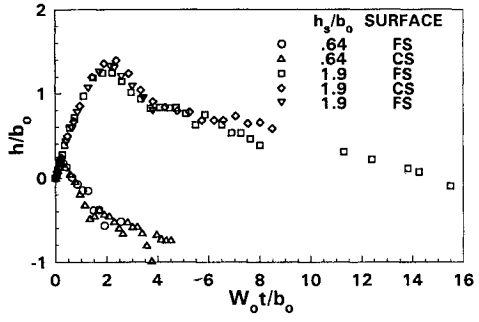

Fig. 3 Ground effects on the vertical translation of a trailing vortex wake.

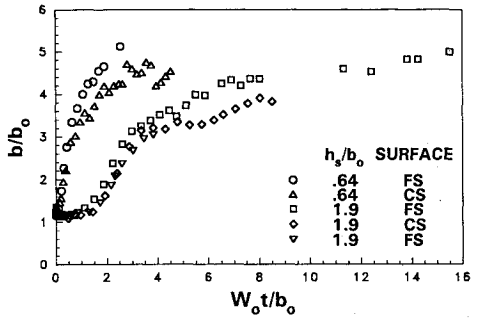

Fig. 4 Ground effects on the vortex separation of a trailing vortex wake.

ment is observed for $W_0t/b_0 < 1$ for $h_s/b_0 = 0.64$ and $W_0t/b_0 < 5$ for $h_s/b_0 = 1.9$.

Comparison of the vortex separation (Fig. 4) shows a similar trend, but the overall agreement is not as good as that of the vertical translation. Reasonably good agreement between the results of the covered and free surfaces is observed for $W_0t/b_0 < 1$ for $h_s/b_0 = 0.64$ and $W_0t/b_0 < 5$ for $h_s/b_0 = 1.9$. There is, however, a distinct difference in the trend of b/b_0 for $h_s/b_0 = 0.64$ and $h_s/b_0 = 1.9$. The vortex separation increases with W_0t/b_0 immediately after the wake is generated for $h_s/b_0 = 0.64$, whereas the separation remains roughly the same until $W_0t/b_0 \approx 1$ before it increases with W_0t/b_0. This indicates that the vortex wake would not be significantly affected by the surface until they were in close proximity.

By the time the maximum vertical translation is reached (i.e., at the time when the surface influence is at its strongest) the vortex separation has increased to about $2b_0$, so both vortices are beyond the open-surface gap and under the foam-covered area. Therefore, there is minimal interaction between the vortex wake and the free surface in the narrow open gap, and the covered surface behaves very much like a rigid surface. From Figs. 3 and 4 it can be seen that the ground effects of interest may be reasonably simulated by either a free or a solid surface.

To further investigate the ground effects on the vortex wake, observations were made of the vortex translation. Figure 5 shows trajectories for $h_s/b_0 = 8.2$, 3.2, 1.9, 1.3, and 0.64. For these runs, the ground surface was simulated by a free surface. The trajectory for $h_s/b_0 = 8.2$ may be considered free of ground effects. According to Sarpkaya and Johnson,[4] the surface has little effect on the vortex wake for $h_s/b_0 > 4.3$. As Fig. 5 illustrates, the trajectories for all runs with $h_s/b_0 \leq 3.2$ show a clear trend of vortex rebound. Initially, the vortex trajectories collapse onto a single curve with that for $h_s/b_0 = 8.2$ as the envelope, as if the water surface were absent. Subsequently, the trajectories deviate from the envelope as the presence of the water surface is felt; the smaller the value of h_s/b_0, the sooner the deviation takes place.

The corresponding trajectories of the vortex separation are shown in Fig. 6. For $h_s/b_0 = 8.2$ (open circles), the vortex separation b/b_0 is initially equal to the wing span S/b_0 or $4/\pi$; it decreases and is maintined at around unity for a while. As a result of the sinusoidal or linking instability,[11] there is a trend of a slight increase in b/b_0 with W_0t/b_0 where this instability is observed; b/b_0 reaches a maximum at about $W_0t/b = 5$ and begins to decrease again. Linking of the vortices takes place at the location of the laser sheet between $W_0t/b_0 = 7$ and 8.[10] For all but the run with $h_s/b_0 = 0.64$, as discussed earlier, the vortex separation follows the trend of that for $h_s/b_0 = 8.2$ initially and begins to increase as the presence of the surface is felt. The rate of increase in b/b_0 increases, and

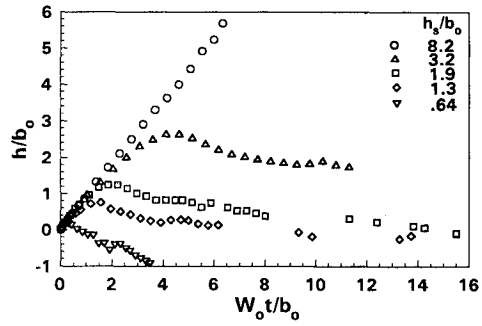

Fig. 5 Ground effects on the vertical translation of a trailing vortex wake for several values of h_s/b_0.

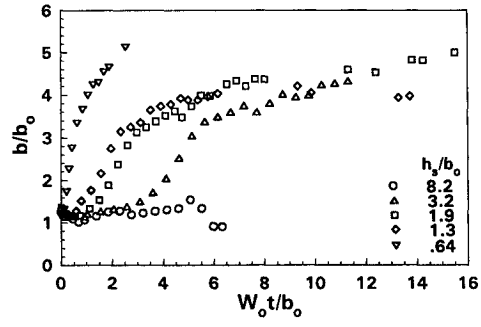

Fig. 6 Ground effects on the vortex separation of a trailing vortex wake for several values of h_s/b_0.

the period of transition before the maximum rate is reached decreases with decreasing h_s/b_0. The time at which the maximum rate of increase is reached corresponds to that at which the maximum vertical translation is reached; therefore, the ground effects are the strongest at this time. Finally, the rate of increase in b/b_0 decreases again after the vortex wake rebounds. At least in one run ($h_s/b_0 = 1.3$) the spread of the vortex cores is arrested after $W_0t/b_0 > 9$. The arrest of the horizontal motion of the vortex pair has been observed by other investigators.[3] From the initial trend established in Fig. 6, it is evident that $h_s/b_0 \approx 1$ is a demarcation below which a vortex wake will feel the presence of the ground immediately.

An immediate consequence of the increase in the vortex separation is the suppression of the linking instability. Under certain circumstances, coherent vortex cores may persist longer than the normal lifespan of the vortex wake (i.e., $W_0t/b_0 < 10$, depending on the ambient turbulence intensity[10]) in the absence of ground effects, which could increase the potential hazard of the vortex wake to following aircraft near ground level.

One of the main concerns in modeling the vortex rebound phenomenon in a towing tank is the influence of the tank sidewalls. The velocity induced by the mirror image of the sidewalls on the main vortex, if sufficiently strong, could result in a rebound phenomenon similar to that caused by ground effects.[4] The dimensionless width of the towing tank is 15, and the initial separation between the tank wall and the vortex cores is 7. For the worst condition, the vortex/wall separation is larger than 5 (see Figs. 5 and 6). Therefore, the influence of the primary vortices at the point of rebound by their surface mirror images (≈0.5 separation) and by their counter-rotating halves (<2.5 separation) overwhelms that of their wall images.

Once the vortex wake feels the presence of the ground, b_0 may no longer be a meaningful length scale. The maximum vertical translation of the vortex wake, as expressed in Eq. (5), may then be considered a logical substitute. To test the validity of such a consideration, we replotted Fig. 5, excluding the trajectory for $h_s/b_0 = 8.2$, in Fig. 7 by replacing b_0 with h_{max} in both the abscissa and ordinate. Comparison of the two figures shows that applying the new length scale h_{max} tends to collapse the three trajectories for $h_s/b_0 = 1.3$ to 3.2, but fails to do so for $h_s/b_0 = 0.64$. The acute, nearly specular rebounding angle differs greatly from those trajectories with larger h_s/b_0.

Figure 8 illustrates the vortex trajectories in a vertical plane perpendicular to the vortex axis. The coordinates of the trajectories y and z are derived from the measurements of h and b shown in Figs. 5 and 6. To conform with Eq. (4), the coordinates are nondimensionalized with b_∞. The symbols represent the experimental results, and the solid curve represents the corresponding theoretical values[1] from Eq. (4). For $h_s/b_0 = 8.2$, the presence of the surface has little influence over the vortex wake before it is disintegrated due to the linking instability. In fact, the evolution of the linking instability results in a relatively large discrepancy between the measured and predicted trajectories. The rest of the experimental results appear to collapse onto a single curve, close to the hyperbolic trajectory for $y/b_\infty < 1$, and then branch out into two distinctive groups, $h_s/b_0 = 1.3$–3.2 and $h_s/b_0 = 0.64$, when $y/b_\infty > 1$.

For $y/b_\infty < 1$, a slight discrepancy is anticipated in the theory due to the idealized representation of trailing vortex wakes by two parallel line vortices. Note that the initial separation measured from the visual results is equal to the span of the

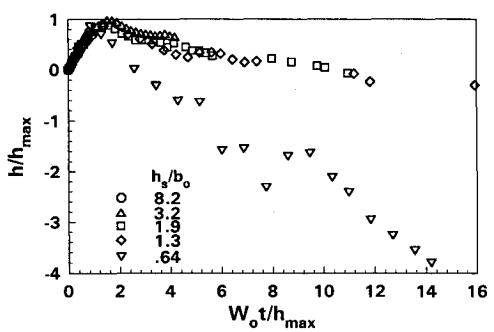

Fig. 7 Ground effects on the vertical translation of a trailing vortex wake where the length scale b_0 is replaced with the maximum translation h_{max}.

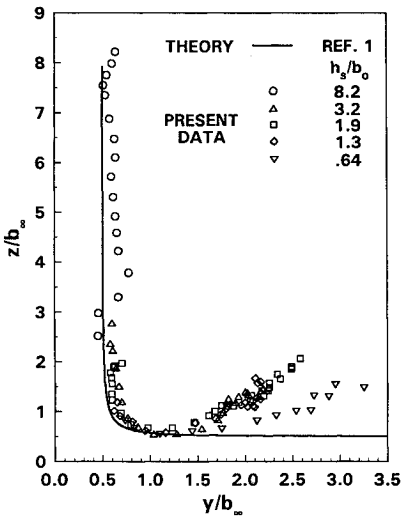

Fig. 8 Comparison of vortex trajectories in ground effect as derived from visual results and classical theory.[1]

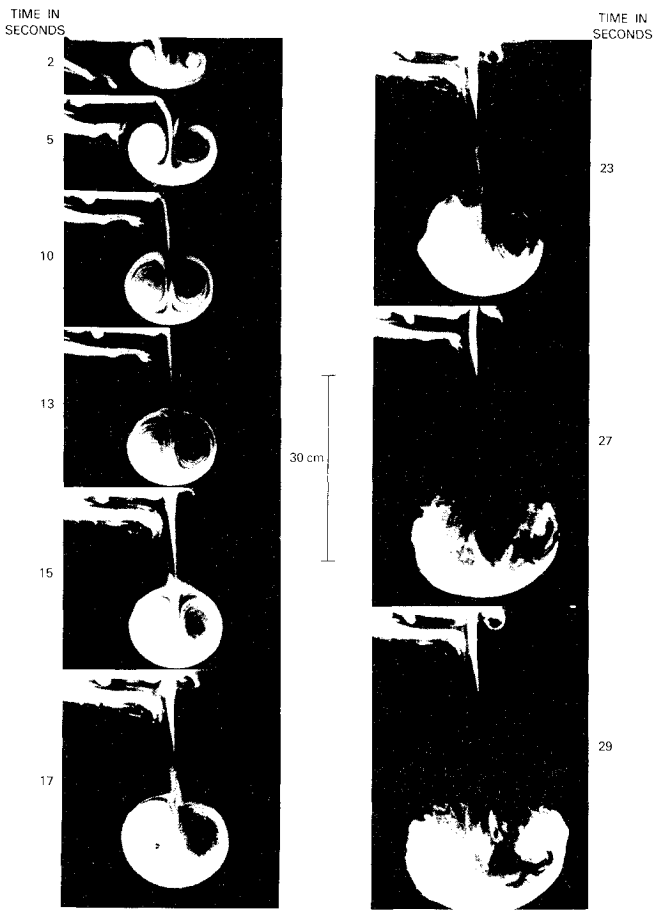

Fig. 9 Evolution of a slotted-jet vortex pair in a homogeneous fluid in the absence of ground effect.

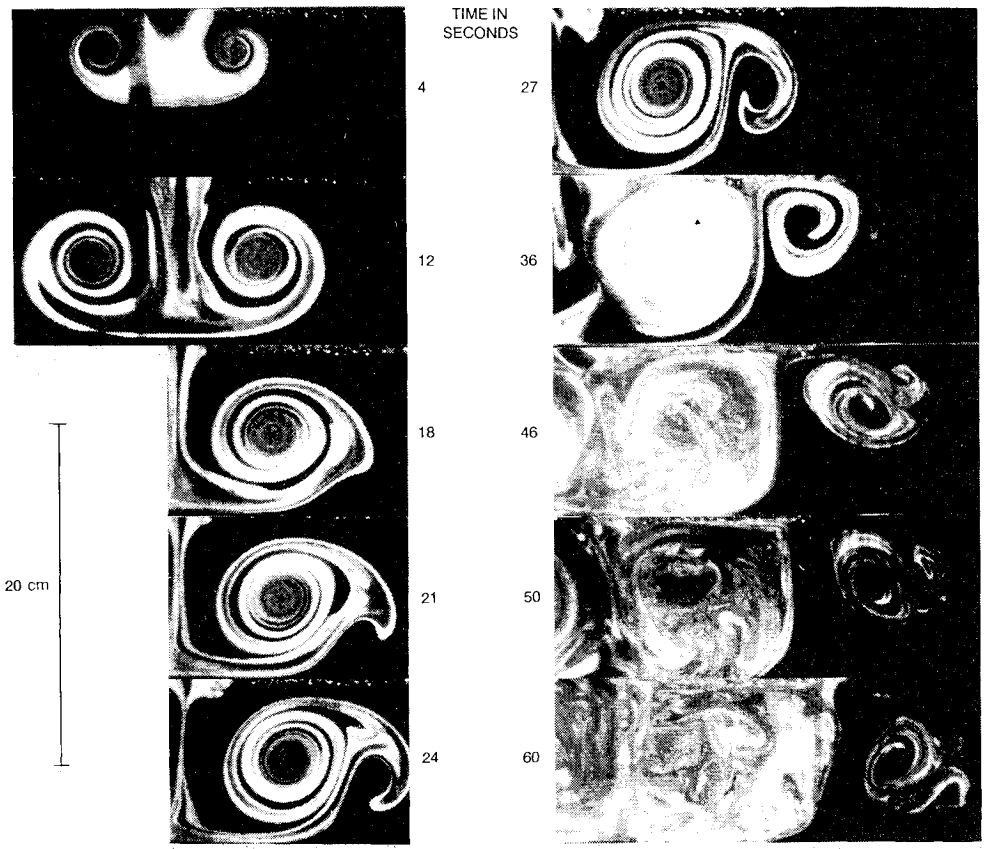

Fig. 10 Generation of secondary vortices and the rebound of the primary slotted-jet vortices, $h_s/b_0 = 1.78$.

wing, which is a factor of $4/\pi$ larger than b_0. The experimental results tend to be above and to the right of the theoretical curve, indicating that the primary vortex is less penetrative than predicted by the two-dimensional theory.

For $y/b_\infty > 1$, the inadequacy of Eq. (2) or (4) in accounting for the rebound of the primary vortex is evident. For $h_s/b_0 = 0.64$, the trajectory is seen to deviate considerably from those at larger h_s/b_0. As shown in Fig. 6, b/b_0 begins to increase immediately after the wake is released, which differs from the trend of the others with larger h_s/b_0. The close proximity of the surface could have resulted in a strong impingement of the vortex pair onto the surface, which may alter the strength of the secondary vortex.

Slotted-Jet Vortex Pair

In an attempt to demonstrate the rebound phenomenon convincingly, the slotted-jet vortex generator was used with a rigid plate made of Plexiglas (1.2 m × 3.2 m) placed below the exit slot to simulate the ground. To establish a reference, Fig. 9 presents a series of photographs showing the evolution of a slotted-jet vortex pair without the plate in place ($h_s/b_0 > 13$). The vortex separation remains about the same until vortex breakdown takes place at $W_0t/b_0 \approx 4.8$. The corresponding slotted-jet vortex pair in ground effect with $h_s/b_0 = 1.78$ is shown in Fig. 10. The vortex separation increases as the vortex pair approaches the surface. The bottom of the oval contacts the surface between $W_0t/b_0 = 0.54$ and 0.81. The formation of a counter-rotating secondary vortex beneath and outboard of the right primary vortex becomes evident at $W_0t/b_0 = 0.81$.

Again, the secondary vortex is not visible in the absence of dye outboard of the primary vortex. The secondary vortex can be identified after dye from the primary vortex is entrained into the recirculation region of the new formation. As soon as the secondary vortex begins to form, rebound of the primary vortex is initiated. The primary and secondary vortices form a vortex pair that moves upward. The top of the oval contacts the bottom of the exit plate of the vortex generator between $W_0t/b_0 = 1.2$ and 1.6. Now, a tertiary vortex is generated outboard and above the secondary vortex. These vortices form another vortex pair that moves away from the primary vortex, which is rapidly disintegrating. Tipping of the vortex pair is clearly observed as it moves away from the bounded region between the two plates (the top plate is only $2.2b_0$ beyond the slot of the generator).

Modified Two-Dimensional Theory

An attempt is made in this section to examine the effects of the secondary vortex on the rebound of the primary vortex. The classical two-dimensional theory, or Eq. (4), is modified by adding a line vortex to account for the secondary vortex.[1] Because the velocity induced by a vortex is inversely proportional to the square of the distance between the vortices, it is assumed that to a first-order approximation, the modification of the trajectory of the primary vortex is due to the effect of the nearest secondary vortex. The total induced velocity of the primary vortex becomes

$$\frac{dy}{dt} = \frac{-\kappa y^2}{4\pi r^2 z} + \frac{\kappa' \cos\theta'}{2\pi r'} \tag{6}$$

$$\frac{dz}{dt} = \frac{-\kappa z^2}{4\pi r^2 y} + \frac{\kappa' \sin\theta'}{2\pi r'} \tag{7}$$

Eqs. (6) and (7), therefore, describe the superposition of a translational velocity due to the four primary vortices (of which two are the mirror image) and the rotational motion induced by the nearest secondary vortex. The differential equation describing the trajectory of the primary vortex is modified to

$$\frac{dz}{dy} = \frac{-\dfrac{z^2}{yr^2} + 2\dfrac{\kappa'}{\kappa}\dfrac{1}{r'}\sin\theta'}{-\dfrac{y^2}{zr^2} + 2\dfrac{\kappa'}{\kappa}\dfrac{1}{r'}\cos\theta'} \tag{8}$$

Note that three additional unknown parameters, κ', r', and θ', were introduced. The angle of rotation of the primary and secondary vortex pair can be expressed as[1]

$$\frac{d\theta'}{dt} = \frac{(\kappa - \kappa')}{2\pi r'^2} \tag{9}$$

Assuming that the secondary vortex is induced at the ground surface, and that the distance r' and vortex strength κ and κ' remain constant, the system of Eqs. (6), (7), and (9) can be numerically computed using the second- and third-order Runge-Kutta algorithm. Four curves corresponding to the conditions $\kappa'/\kappa = 0.3$, 0.7, 0.8, and 0.9 are shown in Fig. 11. In these computations $r' = b_\infty/2$ is assumed. The secondary vortex was assumed to be induced at the matching position when $y/b_\infty = 1.0$ and $z/b_\infty = 0.577$. In the figure, the trajectory given by the classical theory is shown as a solid curve.[1] Note that the trajectories for $\kappa'/\kappa = 0$ and 1 are identical to those computed from the classical theory.

From the comparison of the classical and modified theories in Fig. 11, several interesting features of the vortex system are observed. First, the incorporation of the secondary vortices has brought about the rebound of the primary vortex, which agrees qualitatively with the present experimental results. The trajectories derived from the modified theory show that the rebound motion is periodic; the amplitude and the wavelength depend on the κ'/κ ratio. The periodicity results in momentary arrest of the vortex separation, which is observed experimentally (Fig. 6; see also Ref. 3). The modified theoretical results are in agreement with more elaborate numerical models (e.g., Refs. 9, 12, 13). It should be emphasized that the theory considers two idealized line vortices. In reality, disintensification of the vortex core as a result of diffusion and turbulent mixing would smear the appearance of the periodicity, even if it is present.

The visual results of the trailing vortex pair (Figs. 1 and 2) show that the strength of the secondary vortices is weaker than that of the primary vortices. Therefore, we expect the ratio of κ'/κ to be less than unity. Intuitively, κ'/κ should decrease with increasing h_s/b_0, as the primary vortex disintensifies greatly with the long travel time accompanied by a large h_s/b_0 before impinging onto the ground and initiating the secondary vortex. For the extreme case, the vortex pair released at $h_s/b_0 = 8.5$ does not feel the presence of the ground before it disintegrates. This is consistent with the trend shown in Figs. 8 and 11, except that the periodicity in the solution of the modified theory causes the trajectory for $\kappa'/\kappa = 0.3$ to reverse after a strong initial rebound. Visual results show that the vortex separation between the secondary and primary vortices increases with time as the former spirals around the latter. This also suggests that the periodicity would not be observed in the real fluid.

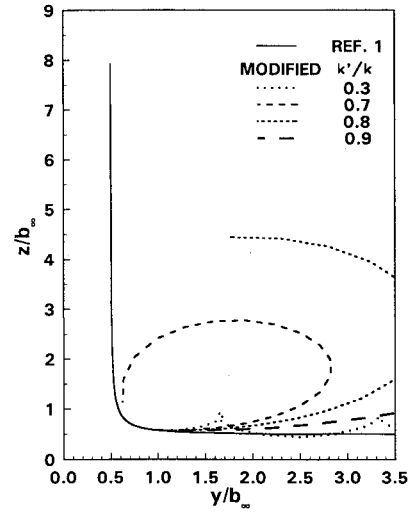

Fig. 11 Comparison of vortex trajectories in ground effect as derived from classical[1] and modified theories.

The good qualitative agreement between the prediction by the modified theory and the experimental results, indicates that the inception of the secondary vortices provides the essential physical mechanism to effect the rebound phenomenon. Accurate prediction must rely on more sophisticated numerical models capable of realistically simulating the viscous-inviscid interaction near the boundary.

Conclusions

Several series of towing tank experiments were conducted to investigate ground effects on vortex wakes. Fluorescent dye was used as a tracer to visualize the evolution of the vortex wakes generated by a towed NACA 0012 wing and by a slotted-jet vortex generator. An argon-ion laser sheet was used to illuminate the vortex wakes. To suspend the towed wing, a unique mounting system consisting of three thin wires was used. The vortex generator was based on an innovative design with a soft stop at the end of the stroke.

The important findings from the laboratory experiments are summarized below:

1) The generation of a secondary vortex outboard of the primary vortex leads to the rebound of the latter from either a free or rigid surface as demonstrated through visual experiments for both a trailing vortex wake and a slotted-jet vortex pair. For the trailing vortex wake, the secondary vortex is relatively weak in strength. As a result, the secondary vortex spirals around the primary vortex and eventually evolves into a patch of turbulence separated from the primary vortex. The vortex separation between the secondary and primary vortices increases with time. For the slotted-jet vortex pair, the secondary vortex appears to have higher strength and longer persistence than that generated by the trailing vortex wake.

2) For trailing vortex wakes, the trajectories for the vortex translation and separation are similar whether the ground is simulated by a free or a rigid surface. This finding is consistent with observations that surface contamination causes the free surface to act like a rigid surface during vortex impingement.[9] Our results have confirmed the scenario inferred by Harvey and Perry[3] where the secondary vortex is due to unsteady separation of the boundary layer in which the flow has to negotiate an adverse pressure gradient created by the impingement of the primary vortex.

3) The vortex separation b/b_0 and the rate of separation are inversely proportional to the ground clearance h_s/b_0. For small values ($h_s/b_0 = 0.64$), b/b_0 increases immediately after the vortex is released, whereas for large values ($h_s/b_0 \geq 1.3$), b/b_0 remains roughly constant before it increases. There is a tendency for the horizontal vortex motion to be arrested at large times. The increase in the vortex separation weakens the linking instability. Under certain circumstances, the swirl in the vortex wake may persist longer than its normal lifespan due to its sinusoidal instability in the absence of ground effect.[10,11]

4) A simple modification of the two-dimensional inviscid theory—namely, adding a secondary vortex to the system—essentially recreates the rebound of the primary vortex, which agrees qualitatively with the experimental results. The rebound curvature appears to reach an asymptotic magnitude when the initial release is sufficiently far from the ground surface. The critical dimensionless distance is approximately one ($h_s/b_0 = 1$). Accurate prediction would require a numerical model capable of simulating the viscous-inviscid interaction and turbulent diffusion taking place at the boundary layer.

Acknowledgments

The study was sponsored by the Transportation Systems Center, U.S. Department of Transportation, under SBIR Contract DTRS-57-87-C-0019 and by a QUEST IR&D fund.

The authors thank C.-M. Ho of the University of Southern California for discussions on the free-surface effects.

References

[1]Lamb, H., *Hydrodynamics*, 6th ed., Dover, New York, 1945, pp. 221–224.

[2]Dee, F. S., and Nicholas, O. P., "Flight Measurement of Wing Tip Vortex Motion near the Ground," CP 1065, British Aeronautical Research Council, London, Jan. 1968.

[3]Harvey, J. K., and Perry, F. J., "Flowfield Produced by Trailing Vortices in the Vicinity of the Ground," *AIAA Journal*, Vol. 9, No. 8, 1971, pp. 1659–1660.

[4]Sarpkaya, T., and Johnson, S. K., "Trailing Vortices in Homogeneous and Density-Stratified Media," *Journal of Fluid Mechanics*, Vol. 136, 1983, 85–109.

[5]Bilanin, A. J., Teske, M. E., and Hirsh, J. E., "Neutral Atmospheric Effects on the Dissipation of Aircraft Vortex Wakes," *AIAA Journal*, Vol. 16, No. 9, 1978, pp. 956–961.

[6]Barker, S. J., and Crow, S. C., "The Motion of Two-Dimensional Vortex Pairs in a Ground Effect," *Journal of Fluid Mechanics*, Vol. 82, Pt. 4, 1977, pp. 659–661.

[7]Didden, N., and Ho, C.-M., "Unsteady Separation on a Boundary Layer Produced by an Impinging Jet," *Journal of Fluid Mechanics*, Vol. 160, 1985, pp. 235–256.

[8]Rizk, M. H., and Menon, S., "Large-Eddy Simulation of Axisymmetric Excitation Effects on a Row of Impinging Jets," *Physics of Fluids*, Vol. 31, No. 7, 1988, pp. 1892–1903.

[9]Bernal, L. P., Hirsa, A., Kwon, J. T., and Willmarth, W. W., "On the Interaction of Vortex Rings and Pairs with a Free Surface for Varying Amounts of Surface Active Agent," *Physics of Fluids A.*, Vol. 1, No. 12, 1989, pp. 2001–2004.

[10]Liu, H.-T., "Effects of Ambient Turbulence on the Decay of a Trailing Vortex Wake," QUEST TP 268, 1991; see also, *Journal of Aircraft* (to be published).

[11]Crow, S. C., "Stability Theory for a Pair of Trailing Vortices," AIAA 8th Aerospace Sciences Meeting, AIAA Paper 70-53, New York, Jan. 19–21, 1970.

[12]Ohring, S., and H. J. Lugt, "Interaction of a Viscous Vortex Pair with a Free Surface," *Journal of Fluid Mechanics*, Vol. 227, 1991, pp. 47–70.

[13]Walker, J. D. A., Smith, C. R., Cerra, A. W., and Doligalski, T. L., "The Impact of a Vortex Ring on a Wall," *Journal of Fluid Mechanics*, Vol. 181, 1989, pp. 99–141.